



Published in final edited form as:

Cell Rep. 2019 July 09; 28(2): 312–324.e4. doi:10.1016/j.celrep.2019.06.028.

Atoh1 Directs Regeneration and Functional Recovery of the Mature Mouse Vestibular System

Zahra N. Sayyid¹, Tian Wang¹, Leon Chen¹, Sherri M. Jones², Alan G. Cheng^{1,3,*}

¹Department of Otolaryngology-Head and Neck Surgery, Stanford University School of Medicine, Stanford, CA 94305, USA

²Department of Special Education and Communication Disorders, College of Education and Human Sciences, University of Nebraska, Lincoln, NE 68583, USA

³Lead Contact

SUMMARY

Utricular hair cells (HCs) are mechanoreceptors required for vestibular function. After damage, regeneration of mammalian utricular HCs is limited and regenerated HCs appear immature. Thus, loss of vestibular function is presumed irreversible. Here, we found partial HC replacement and functional recovery in the mature mouse utricle, both enhanced by overexpressing the transcription factor Atoh1. Following damage, long-term fate mapping revealed that support cells non-mitotically and modestly regenerated HCs displaying no or immature bundles. By contrast, Atoh1 overexpression stimulated proliferation and widespread regeneration of HCs exhibiting elongated bundles, patent mechanotransduction channels, and synaptic connections. Finally, although damage without Atoh1 overexpression failed to initiate or sustain a spontaneous functional recovery, Atoh1 overexpression significantly enhanced both the degree and percentage of animals exhibiting sustained functional recovery. Therefore, the mature, damaged utricle has an Atoh1-responsive regenerative program leading to functional recovery, underscoring the potential of a reprogramming approach to sensory regeneration.

Graphical Abstract

This is an open access article under the CC BY-NC-ND license (<http://creativecommons.org/licenses/by-nc-nd/4.0/>).

*Correspondence: aglcheng@stanford.edu.

AUTHOR CONTRIBUTIONS

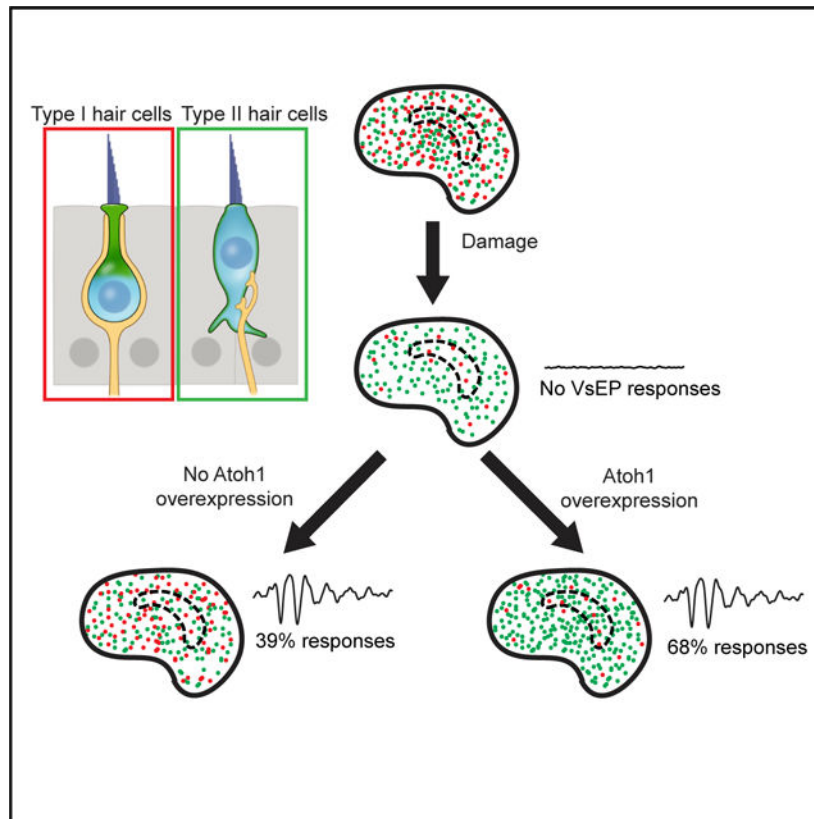
Z.N.S., T.W., S.M.J., and A.G.C. designed experiments. Z.N.S., L.C., T.W., S.M.J., and A.G.C. performed experiments and analyzed data. Z.N.S., T.W., S.M.J., and A.G.C. wrote the manuscript.

SUPPLEMENTAL INFORMATION

Supplemental Information can be found online at <https://doi.org/10.1016/j.celrep.2019.06.028>.

DECLARATION OF INTERESTS

A.G.C. is a scientific advisor for Decibel Therapeutics.



In Brief

The mature mouse utricle, which detects linear acceleration, displays limited regeneration, but whether function returns is unknown. Sayyid et al. show that regenerated hair cells appear and mature over months, resulting in a limited, unsustainable functional recovery. Atoh1 overexpression enhances regeneration and leads to a sustained recovery of vestibular function.

INTRODUCTION

Sensory hair cells (HCs) are essential for vestibular function. In contrast to the cochleae, where no regeneration occurs (Bermingham-McDonogh and Reh, 2011), vestibular organs gradually replace lost HCs (Forge et al., 1993). The mammalian utricle, a vestibular organ that detects linear acceleration, displays new, immature HCs months after damage (Forge et al., 1993, 1998; Kawamoto et al., 2009). However, regeneration occurs almost exclusively in the peripheral zone termed the extrastriola, whereas the central striolar region fails to replace HCs (Golub et al., 2012). Many regenerated HCs bear short stereociliary bundles reminiscent of nascent, immature HCs (Forge et al., 1993; Kawamoto et al., 2009). Although vestibular HCs consist of two subtypes (types I and II), regenerated HCs have been reported to be almost exclusively type II (Bucks et al., 2017; Golub et al., 2012). Because regeneration is limited, loss of vestibular function is at present presumed irreversible.

Unlike the mammalian utricle, support cells in regenerating non-mammalian sensory organs mitotically regenerate both types of vestibular HCs to near complete levels throughout the

organ (Roberson et al., 1992; Weisleder and Rubel, 1992), and function is restored as measured directly via vestibular physiology (Carey et al., 1996; Jones and Nelson, 1992). In mice, although behavior assessment using rotarod testing suggests some improvement of vestibular function months after injury (Schlecker et al., 2011), guinea pigs damaged by aminoglycosides failed to recover function as measured by vestibular evoked potential (VsEP) responses (Bremer et al., 2014). Therefore, it is unclear whether mammalian vestibular HC regeneration leads to restoration of function.

One proposed mechanism to enhance HC regeneration is via overexpression (OE) of Atoh1, a basic-helix-loop-helix transcription factor required for differentiation of developing HCs (Bermingham et al., 1999). In the developing cochlea and utricle, Atoh1 OE induced ectopic HC formation *in vivo* (Gao et al., 2016; Kelly et al., 2012; Liu et al., 2012). On the other hand, several studies have found limited to no ectopic HC formation after Atoh1 OE in the mature cochlea and utricle *in vivo*, indicating an age-related decline in Atoh1 responsiveness (Atkinson et al., 2014; Gao et al., 2016), which may be enhanced *in vitro* or after damage (Schlecker et al., 2011; Shou et al., 2003). In addition, HCs normally downregulate Atoh1 as they mature (Lanford et al., 2000), and constitutive Atoh1 OE in the cochlea prevents maturation (Liu et al., 2012). At present, it remains unclear whether transient or constitutive Atoh1 OE is effective in inducing HC regeneration and functional recovery in the mature mammal.

Here, we show that HCs regenerate and partially mature in the damaged, mature utricle, where Atoh1 OE stimulated proliferation of support cells and regeneration of HCs displaying elongated stereocilia and open mechanotransduction channels. Moreover, Atoh1 OE animals demonstrated more robust VsEP responses relative to damage-only animals. Thus, the damaged, mature mammalian utricle is uniquely competent to respond to Atoh1 OE to enhance both the number and maturation of regenerated HCs, resulting in improved vestibular function.

RESULTS

HCs Spontaneously Regenerate in the Mature Mouse Utricle

We first developed and characterized a damage protocol using the vestibulotoxin IDPN (3,3'-iminodipropionitrile) (Soler-Martin et al., 2007). We administered IDPN to postnatal 30-day-old (P30) mice, an age when utricular function is deemed mature (Jones and Jones, 1999), and found that a moderate dose (4 mg/g) caused 68.2% and 76.3% HC loss in the extrastriola and striola, respectively, 7 days later (Figure 1A; Figures S1A–S1C).

VsEPs (vestibular evoked potentials) are compound action potentials elicited by linear acceleration in the naso-occipital axis (Jones et al., 2001, 2011). Threshold, latency, and amplitude of each waveform represent the overall organ sensitivity, timing of neural transmission, and size and synchrony of the activated neuronal population, respectively (Nazareth and Jones, 1998). Mutant mice with deficient stereociliary bundles or with HC loss demonstrate elevated thresholds, prolonged latencies, and decreased amplitudes (Geng et al., 2009; Krey et al., 2016), indicating that functional HCs are critical for VsEP responses. Seven days after IDPN treatment, animals demonstrated no detectable responses

(Figure 1B). Overall, IDPN-treated animals showed significantly elevated thresholds, longer latencies, and smaller amplitudes compared with undamaged controls (Figure 1C; Figures S1D and S1E). Thus, IDPN treatment effectively decreased HC survival and abolished utricular function.

To assess for HC regeneration, we examined IDPN-treated animals with no detectable VsEP thresholds and found a gradual repopulation of HCs in the extrastriola but not the striola 30–180 days later (Figure 1D; Figure S1F), a finding consistent with other damage paradigms (Golub et al., 2012; Lin et al., 2011). Extrastriolar HC density increased from 29.3% of age-matched controls at 7 days to 56.8% at 180 days after damage (Table S1). Overall, total HC counts increased from 21.8% of age-matched controls at 7 days to 47.8% at 180 days (Figure 1F).

To label newly regenerated HCs, we traced support cells using *Plp1^{CreERT+}*; *Rosa26^{tdTomato/+}* mice (Plp1-Tomato; Figure 1E). After IDPN administration at P30 to ablate HCs, tamoxifen was given at P32 to activate Cre recombinase in support cells, labeling 75.0% of extrastriolar and 45.0% of striolar Sox2⁺ support cells in both undamaged and damaged organs (Figures S2A and S2B). In the undamaged utricle, we found rare tdTomato⁺, Myosin7a⁺ HCs post-tamoxifen injection, corroborating previous reports of rare HC turnover (Figure S2C; Bucks et al., 2017). Seven days post-IDPN treatment, many traced support cells but no traced HCs were found. Mice injected with vehicle control without tamoxifen had minimal recombination (<1%) post-IDPN injection, indicating a low Cre recombinase leakiness as previously reported (Figure S2D; McGovern et al., 2017). After damage, traced HCs significantly increased in the extrastriola over time (Figures 1G and 1H; Figure S2E). In the striola, the increase in traced HCs was small, and the total number of HCs did not significantly increase over time (Figure S2E; Table S1). Together, these data indicate that support cells, particularly those in the extrastriola, contribute to HC regeneration in the mature, damaged mouse utricle.

Atoh1 Enhances HC Regeneration

During development, the transcription factor Atoh1 is essential for HC specification, and expression is downregulated postnatally (Bermingham et al., 1999; Lanford et al., 2000). In the undamaged mature utricle, HCs and support cells rarely express Atoh1 (fewer than two cells per 10,000 μm^2) (Figure S3A). Atoh1 was upregulated in support cells 7–14 days after IDPN treatment (Figures S3B and S3D). We postulated that incomplete, spontaneous regeneration is attributed to insufficient Atoh1 upregulation and hypothesized that Atoh1 OE could enhance HC regeneration. To test this, we used *Plp1^{CreERT+}*; *CAG^{flox-Atoh1-HA/+}* (henceforth Plp1-Atoh1-HA) mice (Liu et al., 2012), in which tamoxifen injection induces constitutive Atoh1 OE in support cells, which are in turn fate-mapped via the hem-agglutinin (HA) tag (Figure 2A). Littermate controls sharing the same genetic background were used as damage-only controls.

Without damage, tamoxifen rarely induced Atoh1-HA expression and failed to stimulate ectopic HC formation (Figures S3E–S3H), despite robust Cre activation as detected by tdTomato expression (Figure S3I). In contrast, tamoxifen induced robust Atoh1-HA expression in support cells in the damaged utricle (Figure S4A; Table S2). Moreover,

significantly more regenerated HCs were observed over time, reaching 80.4% of undamaged, age-matched controls 180 days post-damage (Figures 2B and 2C). Although HCs regenerated mainly in the extrastriola of damage-only utricles (Figures 2D and 2E; Table S1), Atoh1 OE, damaged utricles showed significantly more HCs in both the extrastriola and striola (Figures 2D–2F; Table S1), resulting in significantly more HCs overall.

Atoh1 OE, damaged utricles showed a gradual and significant increase in traced, HA⁺ HCs over time (Figures 2D–2F; Tables S1 and S2), suggesting that Atoh1 OE increased support cell conversion into HCs only after damage. In support of this notion, Atoh1 OE significantly increased Atoh1⁺ support cells only after damage (Figures S3B–S3D). Together, these results suggest that support cells in the damaged, mature utricle are competent to respond to Atoh1 OE and regenerate more HCs.

Atoh1 OE Increases Proliferation

The mature mammalian utricle is mitotically quiescent and remains so after damage. To assess for proliferation early (1 week) and late (1–3 months) post-damage, we immunostained for Ki67 or injected EdU intraperitoneally 3 days per week for 4 weeks. We detected almost no labeled support cells in either damage-only or Atoh1 OE undamaged utricles (Figures 2G–2I; Table S3). By contrast, Atoh1 OE, damaged utricles had Ki67⁺/Sox2⁺ (4.4 ± 9.6 per utricle, $n = 10$) and EdU⁺/Sox2⁺ (20.9 ± 37.3 , $n = 19$) support cells primarily in the striola 30 days post-damage (Figure 2J; Figure S4B). Overall, among the 19 utricles analyzed 30 days post-damage and Atoh1 OE, 7 showed proliferating cells, with a small subset of EdU⁺ cells expressing Myosin7a (Figure 2J). Significantly more EdU⁺/Sox2⁺ support cells were found in Atoh1 OE, damaged utricles than in damage-only utricles (0.0 ± 0.0 , $n = 3$, $p < 0.05$). Most EdU⁺ cells were not tdTomato or HA labeled (Figure 2J; Figures S4B and S4C), suggesting that Atoh1 may have stimulated proliferation in a non-cell-autonomous manner. Ninety days after damage and Atoh1 OE, many EdU⁺/Sox2⁺ but no Ki67⁺/Sox2⁺ cells were found (Figure 2K), suggesting that mitotic cells did not degenerate and mitosis was transient. These data demonstrate that Atoh1 OE induces support cell proliferation of the damaged mouse utricle.

Atoh1 Enhances Stereociliary Bundle Formation

HCs are equipped with stereociliary bundles that lengthen as they mature (Geleoc and Holt, 2003). Months after injury, the mammalian utricle contains HCs bearing short bundles reminiscent of nascent HCs (Forge et al., 1993). We sought to assess the bundles, a presumed surrogate marker of maturation (Ellwanger et al., 2018), of regenerated HCs by labeling for F-actin post-damage (Figure 3A). The apical surface of undamaged utricles is composed of a sheet of HCs with dense, mature stereociliary bundles (Figure 3B). In contrast, 7 days post-damage, most bundles have disappeared, as >77% of HCs are lost (Figures S5A and S5B). At 30 days, 69.8% of traced, regenerated HCs lacked bundles (i.e., bundleless), while 30.2% displayed a spectrum of bundle maturity, most of which appeared short (Figures 3C, 3F, S5C, and S5D). In contrast, bundles were detected on more traced HCs 90–180 days post-damage (Figures 3C and 3F). In comparison, 83.4% of untraced HCs, which represent surviving HCs and some newly regenerated but untraced HCs, displayed

bundles 30 days after damage (Figure 3G). By 180 days, 96.4% of untraced HCs displayed bundles (Figures 3B and 3G). Thus, our data suggest that the apical maturation of regenerated HCs was incomplete, even after a prolonged recovery post-injury.

Constitutive Atoh1 OE restricts HC maturation in the cochlea, resulting in a lack of terminal differentiation markers and bundle development (Atkinson et al., 2014). To determine whether Atoh1 OE regenerated HCs in the utricle can mature, we first examined Atoh1 OE, undamaged tissues and found no bundle abnormalities (Figure 3D). When examining Atoh1 OE, damaged tissues at 30 days, we found that like damage-only tissues, >50% of traced, regenerated HCs were bundleless (Figures 3E and 3F). Unexpectedly, significantly more Atoh1 OE traced HCs displayed bundles 90 (94.0%) and 180 days (95.5%) post-damage compared with damage-only HCs (Figures 3E and 3F).

To assess for functionality of regenerated HCs, we applied Texas red-tagged gentamicin (GTTR), which selectively permeates mechanotransduction channels (Alharazneh et al., 2011). In Atoh1 OE, undamaged utricles, 83.8% of HCs were GTTR⁺, and no HA⁺ HCs were detected (Figures 3H and 3J). In contrast, numerous HA⁺ HCs were present throughout the Atoh1 OE, damaged utricle (Figure 3I), in which 64.6% of Myosin7a⁺/HA⁻ HCs and 32.6% of Myosin7a⁺/HA⁺ incorporated GTTR (Figures 3I and 3J). Taken together, these data suggest that Atoh1 OE regenerated HCs matured and gained the ability to take up GTTR, indicative of patent mechanotransduction channels. Moreover, Atoh1 OE promotes the development of mature-appearing bundles in regenerated HCs.

Regenerated HCs Differentiate into HC Subtypes

The mature mouse utricle is composed of two main subtypes of HCs, estimated to be 55% type I and 45% type II (Desai et al., 2005). Type I HCs express osteopontin (OPN) at the apical neck and are innervated by flask-shaped calyces, whereas type II HCs express a membranous pattern of annexin A4 (ANXA4) and are innervated by boutons (Figure 4C; McInturff et al., 2018). We found that progressively more traced HCs expressed OPN and fewer expressed ANXA4 after damage (Figures 4A, 4D, 4E, 4H, and 4I). By 180 days post-damage, with traced regenerated HCs significantly increased, the proportion of OPN⁺ traced HCs increased, whereas that of ANXA4⁺ traced HCs decreased (Figures 4A, 4D, 4E, 4H, and 4I), suggesting that more HCs with a type I phenotype regenerated over time. In support of this notion, traced HCs associated with Tuj1⁺ calyces increased from 5.5% at 30 days to 12.9% 180 days after damage (Figure 4J; Figure S6A). Altogether, our data suggest that regenerated HCs consist of both type I and type II HCs.

In the Atoh1 OE, damaged utricle, traced HCs predominantly (>93%) expressed the type II HC marker ANXA4 across all time points examined (Figures 4B, 4G, and 4I). Despite an increase in regenerated HCs as a result of Atoh1 OE, the proportion of OPN⁺ traced HCs remained low (Figures 4B, 4F, and 4H). Moreover, traced HCs rarely displayed Tuj1⁺ calyces (Figure 4J). As controls, untraced HCs from damage-only and Atoh1 OE, damaged utricles showed a similar percentage of OPN, ANXA4, and Tuj1 expression across time points (Figures S6B–S6E). All traced, regenerated HCs in both damage-only and Atoh1 OE, damaged utricles were juxtaposed to Tuj1⁺ neurites and appeared innervated. They also had comparable expression of the pre- and post-synaptic markers Ctbp2 and Shank1,

respectively (Figure S6F). These data suggest that Atoh1 OE regenerated HCs acquired a type II HC phenotype at the expense of type I HCs, displayed synaptic elements and appeared innervated.

Atoh1 OE Improves Recovery of Vestibular Function

The avian utricle can regenerate both type I and type II HCs to regain VsEP responses (Jones and Nelson, 1992). We sought to determine whether spontaneous regeneration—in which we have observed a modest regeneration of both type I and type II HCs—or Atoh1-enhanced regeneration—in which we observed type II HC phenotypes, elongated stereociliary bundles, and neural integration—leads to a recovery of vestibular function of the damaged, mature mouse utricle. After initial loss of vestibular function at 7 days, VsEP responses were measured 30, 90, and 180 days after IDPN treatment (Figure 5A). Undamaged, control animals displayed consistent VsEP thresholds at all time points, and Atoh1 OE did not affect thresholds in the undamaged control (Figures 5B and 5C). Many IDPN-treated animals continued to have no measurable response 30 days after damage but regained a partial recovery of responses by 180 days (Figure 5B). These responses, however, remained abnormal as thresholds were higher, latencies longer, and amplitudes smaller than those of age-matched controls (Figures 5B and 5C; Figures S7B and S7C).

Average VsEP thresholds significantly improved from 7–180 days after IDPN treatment but remained significantly higher than undamaged control levels (Figure 5C). After an initial improvement 30–90 days post-damage, average thresholds of damage-only animals worsened at 180 days, suggesting that improvement in responses may be temporary and unsustainable over time. In comparison, average thresholds of Atoh1 OE, damaged animals were significantly better than damage-only animals at 180 days (Figure 5C). Additionally, significantly more Atoh1 OE, damaged animals displayed VsEP responses at 180 days than damage-only animals (Figure 5D).

Both latencies and amplitudes significantly improved over time but remained significantly worse than age-matched controls in both damage-only and Atoh1 OE, damaged animals at 180 days (Figures S7B–S7D), suggesting that the timing of neural transmission was prolonged, and resynchronization of vestibular ganglia firing remained incomplete. Latencies and amplitudes did not significantly differ between damage-only and Atoh1 OE, damaged animals (Figure S7D), suggesting that neural connections of Atoh1 OE regenerated HCs were comparable with those of regenerated HCs in damage-only organs. In support of these results, we detected no gross differences in synaptic protein (Ctbp2 and Shank1) expression in HCs from the two groups (Figure S6F). When comparing HC densities in utricles from individual damaged animals to their corresponding VsEP thresholds, we found a significant correlation (Figures 5E and 5F), suggesting that HC regeneration may have contributed to the functional recovery.

To follow the vestibular function of individual animals over time, we serially measured VsEPs in a subset of animals 7–180 days post-treatment (11 control and 29 damaged for spontaneous regeneration, 5 control and 19 damaged for Atoh1-enhanced regeneration). As expected, all control animals displayed stable thresholds (Figures 5G and 5H). After an initial loss of thresholds in damaged-only animals, we found three trajectories for vestibular

function: (1) no recovery (17.2%), (2) sustained recovery (37.9%), and (3) unsustained recovery (44.8%) as defined by an initial recovery of thresholds followed by a subsequent loss by 180 days (Figure 5G; Table S4). Although >50% of serially analyzed mice recovered VsEP thresholds at 30 and 90 days, <40% of mice had detectable thresholds by 180 days (Figures 5D and 5G). Together, these data suggest that during spontaneous regeneration, 82.8% of animals (24 of 29) are able to partially recover vestibular function, but 54.2% of these animals (13 of 24) failed to recover function in a sustained manner. Among the 19 Atoh1 OE, damaged mice, 21.1% demonstrated no recovery, 68.4% sustained recovery, and 10.5% unsustained recovery (Figure 5H; Table S4). In comparison with damage-only animals, significantly more animals showed a sustained recovery of VsEP responses (Figure 5I). In sum, the mature mouse utricle can partially regain function following damage, but the recovery is commonly unsustained. In contrast, Atoh1 OE leads to a sustained recovery of vestibular function.

DISCUSSION

The mature mammalian cochlea fails to regenerate lost HCs, leading to permanent hearing loss. Although HCs regenerate in the mature mammalian vestibular organs (Forge et al., 1993; Golub et al., 2012; Li et al., 1995; Warchol et al., 1993), whether this limited degree of regeneration leads to a recovery of vestibular function was previously unknown. Here, we demonstrate that the mature mouse utricle is capable of spontaneous and modest regeneration of HCs and recovery of vestibular function over a 6 month time course. Moreover, functional recovery was in part unsustained, leading to a detectable VsEP response in <40% of animals 180 days post-damage. Atoh1 OE significantly increased HC regeneration throughout the utricle, stimulated proliferation, and promoted bundle formation. Overall, Atoh1 OE improved VsEP responses leading to sustained functional recovery in more animals (Figure S8). Collectively, we have revealed that Atoh1 OE promotes vestibular regeneration and functional recovery.

Incomplete Bundle Maturation in Regenerated HCs

We found that regenerating HCs displayed nascent or no bundles, starkly contrasting their more mature basolateral features (HC subtype markers, synaptic proteins, and nerve terminals). In the developing utricle, specified HCs first acquire bundles and mechanotransduction and subsequently basolateral potassium currents and nerve terminals characteristic of HC subtype specialization (Geleoc et al., 2004). Therefore, unlike developing HCs, apical bundles in regenerating HCs fail to mature despite grossly normal synaptic elements and innervation (Atkinson et al., 2015; Zheng and Zuo, 2017; Wang et al., 2019). Such discrepancies in the degrees of maturation of bundles and basolateral features were previously observed in ectopic HCs in the neonatal and mature cochlea and HCs derived from embryonic stem cells (Gubbels et al., 2008; Oshima et al., 2010; Walters et al., 2017).

Damage-Induced Atoh1 Responsiveness

Atoh1 induces ectopic HC formation in the immature cochlea and utricle (Gao et al., 2016; Kelly et al., 2012; Liu et al., 2012). However, the efficacy of Atoh1 in the mature inner ear is

rather limited, as the few Atoh1 OE HCs failed to mature (Atkinson et al., 2014; Liu et al., 2012). After damage, the mature cochlea remains minimally responsive to Atoh1 (Atkinson et al., 2014; Liu et al., 2012). Our results indicate that the damaged mature utricle, but not the undamaged organ, is competent to respond to Atoh1 OE.

Atoh1-HA was rarely detected in the undamaged utricle, but HA-negative cells could be expressing HA at low levels, as HA immunostaining is less sensitive than tdTomato expression. Higher Atoh1-HA levels in the Atoh1 OE, damaged organs may have increased regeneration by enhancing endogenous Atoh1 levels, as the two can correlate at transcription levels during regeneration (Yamashita et al., 2018). Further investigation examining transcription factor networks in the damaged mature utricle can help identify mechanisms of Atoh1 responsiveness.

Multiple Effects of Atoh1 OE on Vestibular Regeneration

Constitutive expression of Atoh1 stimulates ectopic HC formation, yet new HCs fail to fully mature, presumably because of a lack of Atoh1 downregulation (Liu et al., 2012; Yamashita et al., 2018). Our data suggest that sustained Atoh1 OE enhances, rather than prevents, apical maturation of regenerating HCs. Forced expression of Atoh1 was previously reported to induce bundle repair in noise-damaged cochlear HCs (Yang et al., 2012), lending additional evidence that Atoh1 OE can promote bundle formation.

Atoh1 OE also stimulated support cell proliferation, a response previously noted in the neonatal mouse and avian cochlea (Kelly et al., 2012; Lewis et al., 2012). Proliferative cells primarily occupied the striola, suggesting regional differences in proliferative capacity. Previous work on the neonatal mouse utricle showed that damage induced cell cycle re-entry in Lgr5⁺ striolar support cells (Wang et al., 2015). Because most proliferative cells were not traced, Atoh1 OE may have stimulated mitosis in a non-cell-autonomous manner while promoting HC specification and maturation in a cell-autonomous fashion. Comparing Atoh1 target genes in vestibular and cochlear tissues (Yamashita et al., 2018) should shed light on possible mechanisms differentiating their responsiveness.

The degree of HC regeneration induced by Atoh1 OE exceeds that of spontaneous regeneration, although it remained incomplete relative to undamaged tissues. Because our transgenic approach constitutively introduced a single, extra copy of Atoh1, it is possible that other strategies to overexpressing Atoh1 (e.g., transient and/or multiple copies of Atoh1) may induce different effects.

Vestibular Regeneration and Function

VsEP responses are thought to originate largely from the activation of type I HCs because of their larger conductances (Kim et al., 2011). However, during avian vestibular regeneration, responses return within 7–14 days after damage, when predominantly type II HCs with nascent stereociliary bundles repopulate the epithelium and before type I HCs emerge (Dye et al., 1999; Jones and Nelson, 1992; Weisleder et al., 1990). In our study, Atoh1 OE enhanced regeneration of predominantly type II HCs, leading to improved, sustained functional recovery. This suggests that utricles containing mainly type II HCs may also function to detect linear acceleration and contribute to VsEP responses. In both spontaneous

and Atoh1-enhanced regeneration, HC number correlated with vestibular responses. However, we did not observe a threshold of HC number above which vestibular function more readily recovers.

In the late phase of recovery of vestibular function, we propose that unsustained recovery may have resulted from dysfunction and subsequent loss of regenerated HCs. Regenerating HCs may be susceptible to delayed degeneration, a phenomenon previously observed in the regenerating neonatal cochlea (Atkinson et al., 2018; Cox et al., 2014). Alternatively, insufficient levels of Atoh1 may have caused unsustained recovery during regeneration, and Atoh1 OE may have promoted the maturation and survival of regenerated HCs, which in turn converted animals with unsustained recovery to a sustained recovery pattern. Moreover, the recovery of surviving HCs, striolar HC regeneration and support cell proliferation as a result of Atoh1 OE may have also contributed to improved vestibular function. Other potential contributing factors to the recovery of vestibular function include changes in innervation and synapse formation. In addition to causing HC damage, IDPN is also a neurotoxin targeting neurons in the central and peripheral vestibular systems (Llorens et al., 2011), possibly causing some variability of VsEP results. Our current model is ideal to further investigate the significance of each component in future works.

Our study posits Atoh1 as a promising candidate target to induce regeneration of vestibular sensory organs to restore function. As bona fide HC progenitors, support cells in the damaged mature utricle may reveal factors conferring Atoh1 responsiveness, which should guide future reprogramming approaches for inner ear regeneration.

STAR★METHODS

LEAD CONTACT AND MATERIALS AVAILABILITY

Further information and requests for resources and reagents should be directed to and will be fulfilled by the Lead Contact, Alan Cheng (aglcheng@stanford.edu).

EXPERIMENTAL MODEL AND SUBJECT DETAILS

Mice

Plp1-CreERT (Jackson Laboratory, RRID:IMSR_JAX:005975, Bar Harbor, Maine, USA) (Doerflinger et al., 2003; Gomez-Casati et al., 2010; Madisen et al., 2010), *Rosa26-tdTomato* (Jackson Laboratory, RRID:IMSR_JAX:007908, Bar Harbor, Maine, USA) (Madisen et al., 2010), *CAG-flox-Atoh1-HA* (gift of J. Zuo, Creighton University, Omaha, Nebraska, USA) (Liu et al., 2012), and wild-type CD1 (Charles River, RRID:IMSR_CRL:22, Wilmington, Massachusetts, USA) mice of both sexes were used. Littermates were group housed under standard husbandry conditions and were randomly assigned to experimental groups. All animals were confirmed to be in good health and not involved in previous procedures. Genotypes of experimental animals included: wild-type CD1, *Plp1^{CreERT+}; Rosa26^{tdTomato+}*, *Plp1^{CreERT+}; CAG^{flox-Atoh1-HA+}*, and *Plp1^{CreERT+}; CAG^{flox-Atoh1-HA+}; Rosa26^{tdTomato+}*. IDPN (3,3'-iminodipropioni trile; Pfaltz & Bauer, #I00455, Waterbury, Connecticut, USA) was injected intraperitoneally (IP, 2–6 mg/g) once

for adult mice (P30). Tamoxifen (dissolved in corn oil; #T5648–1G, Sigma-Aldrich, St. Louis, Missouri, USA) (IP, 9 mg/40 g) and EdU (IP, 1 mg/kg, Thermo Fisher Scientific, #A10044, Waltham, Massachusetts, USA) were used in a subset of mice. Mortality was low (< 5%) with the use of multiple drugs (4 mg/g IDPN, tamoxifen, EdU) in transgenic (Plp1-Atoh1-HA) animals. Mortality was ~50% when 6 mg/g IDPN was used. No significant differences in either the degree of damage induced by IDPN or subsequent regeneration were observed between ears or between sexes (data not shown). All protocols conform to relevant regulatory standards and were approved by the Animal Care and Use Committee of the Stanford University School of Medicine and NIH.

METHOD DETAILS

Genotyping

Genomic DNA of transgenic mice was collected to perform PCRs. DNA was isolated by adding 180 μ L of 50 mM sodium hydroxide (NaOH, Thermo Fisher Scientific, S318–500) to ear biopsies, incubating at 98°C for 1 hour, then adding 20 μ L of 1 M Tris-HCl (Invitrogen, Thermo Fisher Scientific, #15568025). A list of primers and sequences used for genotyping can be found in the Key Resources Table.

Vestibular physiology

Linear vestibular evoked potential (VsEP) responses were recorded from mice at various ages (P37, P60, P120, P210) as previously described (Jones and Jones, 1999). Briefly, mice were first anesthetized with a 1:1 cocktail of ketamine (100 mg/kg, #NDC 50989–161-06, Vedco, St. Joseph, Missouri, USA) and xylazine (10 mg/kg, #SC-36294Rx, Santa Cruz Animal Health, Dallas, TX, USA). Rectal temperatures were maintained at 37°C, and electrocardiographic (ECG) activity was monitored using an oscilloscope. Subcutaneous stainless-steel electrodes were placed over the caudal cerebrum (non-inverting electrode), subcutaneously behind the right pinna (inverting electrode), and intramuscularly in the right thigh muscle (ground electrode). A head clip was used to secure the head to the mechanical shaker, which was used to deliver linear vestibular stimuli in the naso-occipital axis. Vertical motion of the shaker was monitored with an accelerometer and adjusted to produce the stimulus waveforms. Throughout the study, jerk stimuli ranging from 0.125 g/ms to 2.0 g/ms were provided (Jones et al., 2011). Signals were amplified (200,000x), filtered (low filter = 300 Hz, high filter = 3000 Hz), and digitized via an analog-to-digital (A/D) converter for all VsEP recordings. Responses from normal and inverted stimulus polarities were collected and added together for a total of 256 sweeps for each waveform. A masker (90 dB SPL; bandwidth 50 Hz to 50 kHz) from a free-field speaker driver was used to prevent responses from the auditory components of cranial nerve VIII. All responses were blindly analyzed for three components: threshold (g/ms), P1 latency (ms) and P1-N1 amplitude (μ V). Thresholds were defined as the average stimulus intensity between the lowest stimulus intensity at which a response was observed and the following stimulus intensity that failed to elicit a response. Latencies were measured relative to the onset of the stimulus for the first positive response peak (P1). Amplitudes represented peak-to-peak magnitudes between P1 and N1. Whereas the first positive and negative response peaks (P1 and N1, respectively) reflect

activity of the peripheral vestibular nerve, peaks beyond N1 reflect activity of the brainstem and central vestibular relays (Jones, 1992; Nazareth and Jones, 1998).

Immunohistochemistry

After microdissection from the temporal bone, utricles were fixed in 4% paraformaldehyde (in PBS, pH 7.4; Electron Microscopy Services, #15710, Hatfield, Pennsylvania, USA) for 40 min at room temperature. Tissues were then washed with PBS 3 times for at least 5 minutes each, then blocked with 5% donkey serum, 0.1% Triton X-100, 1% bovine serum albumin (BSA, Thermo Fisher Scientific, #BP1600–100), and 0.02% sodium azide (NaN_3 , Sigma-Aldrich, #S2002–25G) in PBS at pH 7.4 for 1 hour at room temperature. Primary antibodies diluted in the same blocking solution were added overnight at 4°C. The following day, after washing with PBS, tissues were incubated with secondary antibodies diluted in 0.1% Triton X-100, 0.1% BSA, and 0.02% NaN_3 solution in PBS at pH 7.4 for 2 hours at room temperature. After washing with PBS, tissues were mounted with antifade Fluorescence Mounting Medium (DAKO, Agilent, #S3023, Santa Clara, California, USA) and coverslipped. Antibodies against the following proteins were used: Myosin7a (1:1000, rabbit, RRID:AB_2314839, Proteus Biosciences, Ramona, California, USA), Myosin7a (1:500, mouse, DSHB, RRID:AB_2282417, Iowa City, Iowa, USA), Sox2 (1:400, goat, RRID:AB_2286684, Santa Cruz Biotechnology, Santa Cruz, California, USA), AnnexinA4 (1:200, goat, RRID:AB_2242796, R&D Systems, Minneapolis, Minnesota, USA), Osteopontin (1:200, goat, RRID:AB_2194992, R&D Systems), Tuj1 (1:1000, mouse, Neuromics, RRID:AB_2737114, Edina, Minnesota, USA), Neurofilament (1:1000, chicken, Abcam, RRID:AB_304560, Cambridge, United Kingdom), Ctbp2 (1:1000, mouse, RRID:AB_399431, BD Transduction Laboratories, Franklin Lakes, New Jersey, USA), Shank1 (1:1000, goat, RRID:AB_2301736, Santa Cruz Biotechnology), Ki67 (1:500, rabbit, RRID:AB_302459, Abcam, Cambridge, United Kingdom), Atoh1 (1:2000, rabbit, RRID:AB_10733126, Proteintech, Rosemont, Illinois, USA) (Atkinson et al., 2018), and HA (1:500, rabbit, RRID:AB_307019, Sigma-Aldrich). Secondary antibodies included Alexa Fluor donkey anti-goat 488 (RRID:AB_2534102), Alexa Fluor donkey anti-goat 546 (RRID:AB_142628), Alexa Fluor donkey anti-goat 647 (RRID:AB_141844), Alexa Fluor donkey anti-mouse 488 (RRID:AB_141607), Alexa Fluor donkey anti-mouse 546 (RRID:AB_2534012), Alexa Fluor donkey anti-mouse 647 (RRID:AB_162542), Alexa Fluor donkey anti-rabbit 488 (RRID:AB_2535792) Alexa Fluor donkey anti-rabbit 546 (RRID:AB_2534016), Alexa Fluor donkey anti-rabbit 647 (RRID:AB_2536183, all Thermo Fisher Scientific) at 1:250 to 1:500. Fluorescence-conjugated phalloidin (1:1,000; RRID:AB_2620155, Thermo Fisher Scientific), DAPI (1:10,000 from 5mg/ml stock solution; RRID:AB_2629482, Thermo Fisher Scientific), and Alexa Fluor 647 EdU Detection Kit (#C10340, Thermo Fisher Scientific) were used. Texas Red-conjugated gentamicin (GTTR) was synthesized as previously described and applied at 1:200 of stock solution (0.85 mg/mL) for 2 hours (Myrdal et al., 2005; Sandoval et al., 1998).

QUANTIFICATION AND STATISTICAL ANALYSIS

Image acquisition and cell quantification

Low-magnification images were acquired using epifluorescent microscopy (Axioplan 2, Zeiss, Oberkochen, Germany). High-magnification Z stack images were captured using a 63x objective on a Zeiss LSM 700 or 880 confocal microscope (Zen Black, Zeiss). Whole utricle images were acquired using tile scanning via Z-stack images tiled across the length and width of the entire utricle at 63x magnification on the Zeiss LSM 880 confocal microscope. Once the image was captured with Zen Black, it was transferred to Zen Blue for image processing. The image was then stitched during post-processing to fuse the individual tiles. From these Z stack images, cell quantification was performed either per 10,000 μm^2 or per organ using Fiji software (v2.0.0, NIH, Bethesda, Maryland, USA). Cell counts were analyzed either from 1–2 representative areas from the extrastriola and striola, or from merged images spanning the whole utricle (merged together using Zeiss Zen software). Quantification of total HC numbers represents cell counts from the entire sensory epithelium. For all experiments, *n* values represent the number of animals or utricles or cells examined.

Statistical analyses

Statistical analyses were conducted using GraphPad Prism (v7.0c software, GraphPad, San Diego, CA, USA) and RStudio (v0.99.891, RStudio, Inc., Boston, MA, USA). Statistical significance was determined using χ^2 tests, Student's *t* tests, or one- or two-way ANOVA followed by post hoc analysis via Tukey's multiple comparisons test unless otherwise stated as appropriate. A *p* value less than 0.05 was considered significant: **p* < 0.05, ***p* < 0.01, ****p* < 0.001. Data are shown as mean \pm s.d. Linear regression analysis was performed to quantify goodness of fit via computation of the Pearson correlation coefficient (RStudio). Details of experiments can be found in the figures and figure legends. Numbers of animals, utricles, or HCs listed in parentheses.

Supplementary Material

Refer to Web version on PubMed Central for supplementary material.

ACKNOWLEDGMENTS

We thank our lab members, R. Nusse, S. Heller, and J. Raymond for fruitful discussion, W. Dong, M. O'Sullivan, N. Grillet, D. Hosseini, Y. Ma, S. Vijaya-kumar, K. Hotovy, and M. Rosdail for excellent technical support, C. Galapp for illustration, and J. Zuo for mouse sharing. This work was supported by the Stanford Medical Scholars Research Program, Howard Hughes Medical Institute Medical Fellows Program, Stanford MSTP, and NIH/National Institute on Deafness and Other Communication Disorders (NIDCD) grant F30DC015698 (Z.N.S.); the Lucile Packard Foundation for Children's Health and Stanford NIH/National Center for Advancing Translational Sciences (NCATS) Clinical and Translational Science Award (CTSA) UL1 TR001085; the Child Health Research Institute of Stanford University and NIH/NIDCD grant R21DC015879 (T.W.); Nebraska Tobacco Settlement Biomedical Research Development Funds (S.M.J.); and NIH/NIDCD grants K08DC011043, RO1DC013910, and RO1DC016919, Department of Defense grant MR130316, the Akiko Yamazaki and Jerry Yang Faculty Scholar Fund, and California Institute for Regenerative Medicine grants RN3-06529 and DISC2-10537 (A.G.C.).

REFERENCES

- Alharazneh A, Luk L, Huth M, Monfared A, Steyger PS, Cheng AG, and Ricci AJ (2011). Functional hair cell mechanotransducer channels are required for aminoglycoside ototoxicity. *PLoS ONE* 6, e22347. [PubMed: 21818312]
- Atkinson PJ, Wise AK, Flynn BO, Nayagam BA, and Richardson RT (2014). Hair cell regeneration after ATOH1 gene therapy in the cochlea of profoundly deaf adult guinea pigs. *PLoS ONE* 9, e102077. [PubMed: 25036727]
- Atkinson PJ, Huarcaya Najarro E, Sayyid ZN, and Cheng AG (2015). Sensory hair cell development and regeneration: similarities and differences. *Development* 142, 1561–1571. [PubMed: 25922522]
- Atkinson PJ, Dong Y, Gu S, Liu W, Najarro EH, Udagawa T, and Cheng AG (2018). Sox2 haploinsufficiency primes regeneration and Wnt responsiveness in the mouse cochlea. *J. Clin. Invest* 128, 1641–1656. [PubMed: 29553487]
- Birmingham NA, Hassan BA, Price SD, Vollrath MA, Ben-Arie N, Eatock RA, Bellen HJ, Lysakowski A, and Zoghbi HY (1999). Math1: an essential gene for the generation of inner ear hair cells. *Science* 284, 1837–1841. [PubMed: 10364557]
- Birmingham-McDonogh O, and Reh TA (2011). Regulated reprogramming in the regeneration of sensory receptor cells. *Neuron* 71, 389–405. [PubMed: 21835338]
- Bremer HG, Versnel H, Hendriksen FG, Topsakal V, Grolman W, and Klis SF (2014). Does vestibular end-organ function recover after gentamicin-induced trauma in Guinea pigs? *Audiol. Neurotol* 19, 135–150.
- Bucks SA, Cox BC, Vlosich BA, Manning JP, Nguyen TB, and Stone JS (2017). Supporting cells remove and replace sensory receptor hair cells in a balance organ of adult mice. *eLife* 6, e18128. [PubMed: 28263708]
- Carey JP, Fuchs AF, and Rubel EW (1996). Hair cell regeneration and recovery of the vestibuloocular reflex in the avian vestibular system. *J. Neurophysiol* 76, 3301–3312. [PubMed: 8930274]
- Cox BC, Chai R, Lenoir A, Liu Z, Zhang L, Nguyen DH, Chalasani K, Steigelman KA, Fang J, Cheng AG, et al. (2014). Spontaneous hair cell regeneration in the neonatal mouse cochlea in vivo. *Development* 141, 816–829. [PubMed: 24496619]
- Desai SS, Zeh C, and Lysakowski A (2005). Comparative morphology of rodent vestibular periphery. I. Saccular and utricular maculae. *J. Neurophysiol* 93, 251–266. [PubMed: 15240767]
- Doerflinger NH, Macklin WB, and Popko B (2003). Inducible site-specific recombination in myelinating cells. *Genesis* 35, 63–72. [PubMed: 12481300]
- Dye BJ, Frank TC, Newlands SD, and Dickman JD (1999). Distribution and time course of hair cell regeneration in the pigeon utricle. *Hear. Res* 133, 17–26. [PubMed: 10416861]
- Ellwanger DC, Scheibinger M, Dumont RA, Barr-Gillespie PG, and Heller S (2018). Transcriptional dynamics of hair-bundle morphogenesis revealed with CellTrails. *Cell Rep.* 23, 2901–2914.e13. [PubMed: 29874578]
- Forge A, Li L, Corwin JT, and Nevill G (1993). Ultrastructural evidence for hair cell regeneration in the mammalian inner ear. *Science* 259, 1616–1619. [PubMed: 8456284]
- Forge A, Li L, and Nevill G (1998). Hair cell recovery in the vestibular sensory epithelia of mature guinea pigs. *J. Comp. Neurol* 397, 69–88. [PubMed: 9671280]
- Gao Z, Kelly MC, Yu D, Wu H, Lin X, Chi FL, and Chen P (2016). Spatial and age-dependent hair cell generation in the postnatal mammalian utricle. *Mol. Neurobiol* 53, 1601–1612. [PubMed: 25666161]
- Geleoc GS, and Holt JR (2003). Developmental acquisition of sensory transduction in hair cells of the mouse inner ear. *Nat. Neurosci* 6, 1019–1020. [PubMed: 12973354]
- Geleoc GS, Risner JR, and Holt JR (2004). Developmental acquisition of voltage-dependent conductances and sensory signaling in hair cells of the embryonic mouse inner ear. *J. Neurosci* 24, 11148–11159. [PubMed: 15590931]
- Geng R, Geller SF, Hayashi T, Ray CA, Reh TA, Birmingham-McDonogh O, Jones SM, Wright CG, Melki S, Imanishi Y, et al. (2009). Usher syndrome IIIA gene clarin-1 is essential for hair cell function and associated neural activation. *Hum. Mol. Genet* 18, 2748–2760. [PubMed: 19414487]

- Golub JS, Tong L, Ngyuen TB, Hume CR, Palmiter RD, Rubel EW, and Stone JS (2012). Hair cell replacement in adult mouse utricles after targeted ablation of hair cells with diphtheria toxin. *J. Neurosci* 32, 15093–15105. [PubMed: 23100430]
- Gomez-Casati ME, Murtie J, Taylor B, and Corfas G (2010). Cell-specific inducible gene recombination in postnatal inner ear supporting cells and glia. *J. Assoc. Res. Otolaryngol* 11, 19–26. [PubMed: 19820996]
- Gubbels SP, Woessner DW, Mitchell JC, Ricci AJ, and Brigande JV (2008). Functional auditory hair cells produced in the mammalian cochlea by in utero gene transfer. *Nature* 455, 537–541. [PubMed: 18754012]
- Jones TA (1992). Vestibular short latency responses to pulsed linear acceleration in unanesthetized animals. *Electroencephalogr. Clin. Neurophysiol* 82, 377–386. [PubMed: 1374706]
- Jones TA, and Jones SM (1999). Short latency compound action potentials from mammalian gravity receptor organs. *Hear. Res* 136, 75–85. [PubMed: 10511626]
- Jones TA, and Nelson RC (1992). Recovery of vestibular function following hair cell destruction by streptomycin. *Hear. Res* 62, 181–186. [PubMed: 1429260]
- Jones SM, Jones TA, Bell PL, and Taylor MJ (2001). Compound gravity receptor polarization vectors evidenced by linear vestibular evoked potentials. *Hear. Res* 154, 54–61. [PubMed: 11423215]
- Jones TA, Jones SM, Vijayakumar S, Brugeaud A, Bothwell M, and Chabbert C (2011). The adequate stimulus for mammalian linear vestibular evoked potentials (VsEPs). *Hear. Res* 280, 133–140. [PubMed: 21664446]
- Kawamoto K, Izumikawa M, Beyer LA, Atkin GM, and Raphael Y (2009). Spontaneous hair cell regeneration in the mouse utricle following gentamicin ototoxicity. *Hear. Res* 247, 17–26. [PubMed: 18809482]
- Kelly MC, Chang Q, Pan A, Lin X, and Chen P (2012). Atoh1 directs the formation of sensory mosaics and induces cell proliferation in the postnatal mammalian cochlea in vivo. *J. Neurosci* 32, 6699–6710. [PubMed: 22573692]
- Kim KS, Minor LB, Della Santina CC, and Lasker DM (2011). Variation in response dynamics of regular and irregular vestibular-nerve afferents during sinusoidal head rotations and currents in the chinchilla. *Exp. Brain Res* 210, 643–649. [PubMed: 21369854]
- Krey JF, Krystofiak ES, Dumont RA, Vijayakumar S, Choi D, Rivero F, Kachar B, Jones SM, and Barr-Gillespie PG (2016). Platin 1 widens stereocilia by transforming actin filament packing from hexagonal to liquid. *J. Cell Biol* 215, 467–482. [PubMed: 27811163]
- Lanford PJ, Shailam R, Norton CR, Gridley T, and Kelley MW (2000). Expression of Math1 and HES5 in the cochleae of wildtype and Jag2 mutant mice. *J. Assoc. Res. Otolaryngol* 1, 161–171. [PubMed: 11545143]
- Lewis RM, Hume CR, and Stone JS (2012). Atoh1 expression and function during auditory hair cell regeneration in post-hatch chickens. *Hear. Res* 289, 74–85. [PubMed: 22543087]
- Li L, Nevill G, and Forge A (1995). Two modes of hair cell loss from the vestibular sensory epithelia of the guinea pig inner ear. *J. Comp. Neurol* 355, 405–417. [PubMed: 7636022]
- Lin V, Golub JS, Nguyen TB, Hume CR, Oesterle EC, and Stone JS (2011). Inhibition of Notch activity promotes nonmitotic regeneration of hair cells in the adult mouse utricles. *J. Neurosci* 31, 15329–15339. [PubMed: 22031879]
- Liu Z, Dearman JA, Cox BC, Walters BJ, Zhang L, Ayrault O, Zindy F, Gan L, Roussel MF, and Zuo J (2012). Age-dependent in vivo conversion of mouse cochlear pillar and Deiters' cells to immature hair cells by Atoh1 ectopic expression. *J. Neurosci* 32, 6600–6610. [PubMed: 22573682]
- Llorens J, Soler-Martin C, Saldana-Ruiz S, Cutillas B, Ambrosio S, and Boadas-Vaello P (2011). A new unifying hypothesis for lathyrism, konzo and tropical ataxic neuropathy: nitriles are the causative agents. *Food Chem. Toxicol* 49, 563–570. [PubMed: 20553991]
- Madisen L, Zwingman TA, Sunkin SM, Oh SW, Zariwala HA, Gu H, Ng LL, Palmiter RD, Hawrylycz MJ, Jones AR, et al. (2010). A robust and high-throughput Cre reporting and characterization system for the whole mouse brain. *Nat. Neurosci* 13, 133–140. [PubMed: 20023653]
- McGovern MM, Brancheck J, Grant AC, Graves KA, and Cox BC (2017). Quantitative analysis of supporting cell subtype labeling among CreER lines in the neonatal mouse cochlea. *J. Assoc. Res. Otolaryngol* 18, 227–245. [PubMed: 27873085]

- McInturff S, Burns JC, and Kelley MW (2018). Characterization of spatial and temporal development of type I and type II hair cells in the mouse utricle using new cell-type-specific markers. *Biol. Open* 7, bio038083. [PubMed: 30455179]
- Myrdal SE, Johnson KC, and Steyger PS (2005). Cytoplasmic and intra-nuclear binding of gentamicin does not require endocytosis. *Hear. Res* 204, 156–169. [PubMed: 15925201]
- Nazareth AM, and Jones TA (1998). Central and peripheral components of short latency vestibular responses in the chicken. *J. Vestib. Res* 8, 233–252. [PubMed: 9626650]
- Oshima K, Shin K, Diensthuber M, Peng AW, Ricci AJ, and Heller S (2010). Mechanosensitive hair cell-like cells from embryonic and induced pluripotent stem cells. *Cell* 141, 704–716. [PubMed: 20478259]
- Roberson DF, Weisleder P, Bohrer PS, and Rubel EW (1992). Ongoing production of sensory cells in the vestibular epithelium of the chick. *Hear. Res* 57, 166–174. [PubMed: 1733910]
- Sandoval R, Leiser J, and Molitoris BA (1998). Aminoglycoside antibiotics traffic to the Golgi complex in LLC-PK1 cells. *J. Am. Soc. Nephrol* 9, 167–174. [PubMed: 9527392]
- Schlecker C, Praetorius M, Brough DE, Presler RG Jr., Hsu C, Plinkert PK, and Staecker H (2011). Selective atonal gene delivery improves balance function in a mouse model of vestibular disease. *Gene Ther.* 18, 884–890. [PubMed: 21472006]
- Shou J, Zheng JL, and Gao WQ (2003). Robust generation of new hair cells in the mature mammalian inner ear by adenoviral expression of *Hath1*. *Mol. Cell. Neurosci* 23, 169–179. [PubMed: 12812751]
- Soler-Martin C, Diez-Padrisa N, Boadas-Vaello P, and Llorens J (2007). Behavioral disturbances and hair cell loss in the inner ear following nitrile exposure in mice, guinea pigs, and frogs. *Toxicol. Sci* 96, 123–132. [PubMed: 17159233]
- Walters BJ, Coak E, Dearman J, Bailey G, Yamashita T, Kuo B, and Zuo J (2017). In vivo interplay between p27(Kip1), GATA3, ATOH1, and POU4F3 converts non-sensory cells to hair cells in adult mice. *Cell Rep.* 19, 307–320. [PubMed: 28402854]
- Wang T, Chai R, Kim GS, Pham N, Jansson L, Nguyen DH, Kuo B, May LA, Zuo J, Cunningham LL, et al. (2015). *Lgr5+* cells regenerate hair cells via proliferation and direct transdifferentiation in damaged neonatal mouse utricle. *Nat. Commun* 6, 6613. [PubMed: 25849379]
- Wang T, Niwa M, Sayyid ZN, Hosseini DK, Pham N, Jones SM, Riccio AJ, and Cheng AG (2019). Uncoordinated maturation of developing and regenerating postnatal mammalian vestibular hair cells. *PLoS Biol.* 17, e3000326. [PubMed: 31260439]
- Warchol ME, Lambert PR, Goldstein BJ, Forge A, and Corwin JT (1993). Regenerative proliferation in inner ear sensory epithelia from adult guinea pigs and humans. *Science* 259, 1619–1622. [PubMed: 8456285]
- Weisleder P, and Rubel EW (1992). Hair cell regeneration in the avian vestibular epithelium. *Exp. Neurol* 115, 2–6. [PubMed: 1728567]
- Weisleder P, Jones TA, and Rubel EW (1990). Peripheral generators of the vestibular evoked potentials (VsEPs) in the chick. *Electroencephalogr. Clin. Neurophysiol* 76, 362–369. [PubMed: 1699729]
- Yamashita T, Zheng F, Finkelstein D, Kellard Z, Carter R, Rosencrance CD, Sugino K, Easton J, Gawad C, and Zuo J (2018). High-resolution transcriptional dissection of in vivo *Atoh1*-mediated hair cell conversion in mature cochleae identifies *Isl1* as a co-reprogramming factor. *PLoS Genet.* 14, e1007552. [PubMed: 30063705]
- Yang SM, Chen W, Guo WW, Jia S, Sun JH, Liu HZ, Young WY, and He DZ (2012). Regeneration of stereocilia of hair cells by forced *Atoh1* expression in the adult mammalian cochlea. *PLoS ONE* 7, e46355. [PubMed: 23029493]
- Zheng F, and Zuo J (2017). Cochlear hair cell regeneration after noise-induced hearing loss: Does regeneration follow development? *Hear. Res* 349, 182–196. [PubMed: 28034617]

Highlights

- The mature mouse utricle spontaneously regenerates hair cells and recovers function
- Regenerated hair cells gradually increase and acquire bundles over months
- *Atoh1* overexpression enhances proliferation and type II hair cell regeneration
- *Atoh1* overexpression enhances sustained recovery of vestibular function

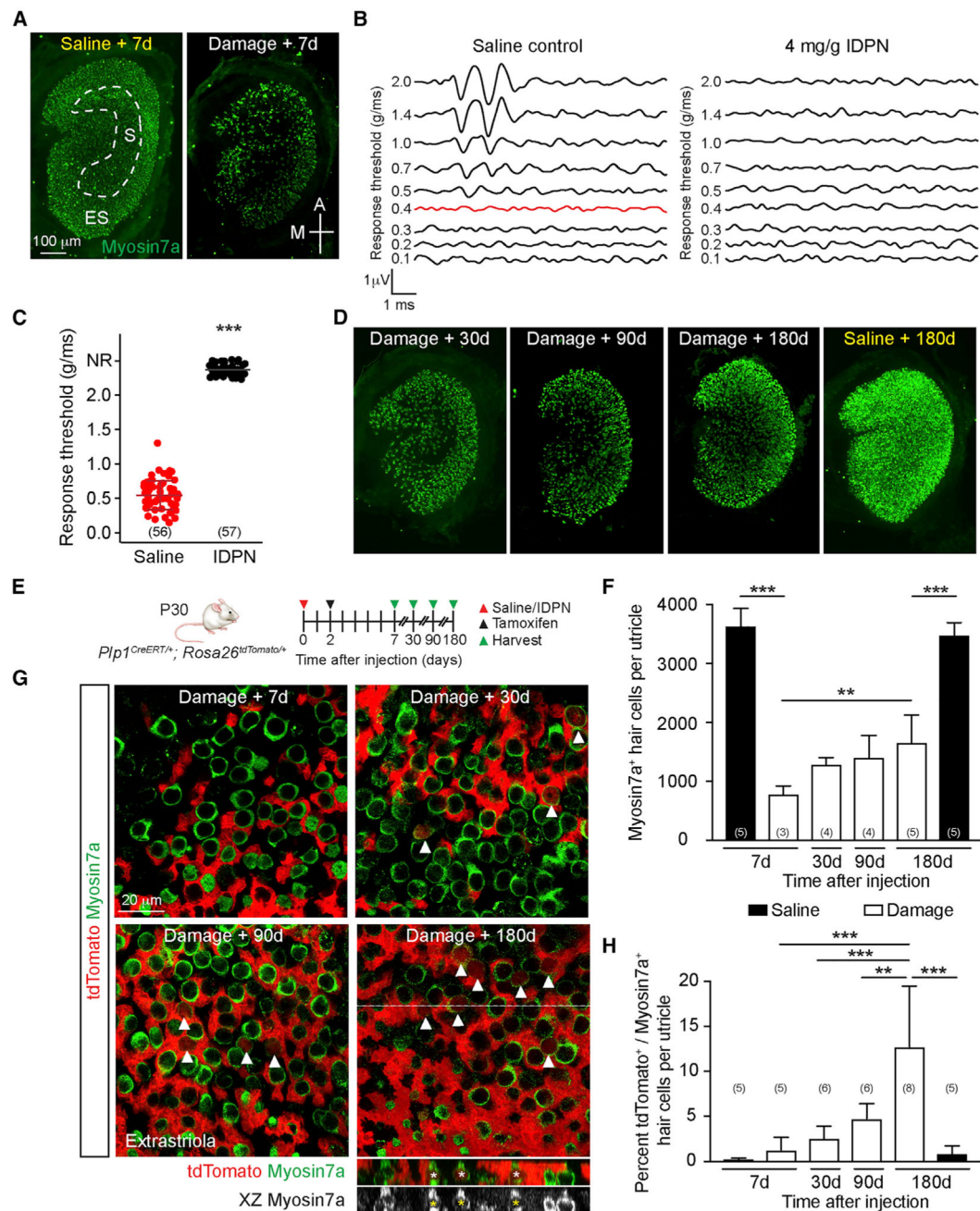


Figure 1. $Plp1^+$ Support Cells Regenerate HCs

- (A) P30 wild-type mice were treated with IDPN, and utricles were examined 1 week later. Undamaged controls were injected with saline. Myosin7a⁺ HCs were identified in the striola (dashed lines) and extrastriola.
- (B) Characteristic VSEP waveforms from undamaged animals (threshold 0.4 g/ms, red) were lost in IDPN-treated animals.
- (C) IDPN-treated animals displayed significantly higher thresholds than undamaged controls.
- (D) Rapid loss followed by gradual repopulation of HCs.

(E) Schematic of transgenic approach to trace support cells.

(F) Quantification shows significant increase in total HC number in the entire organ by 180 days after damage.

(G) Traced HCs increase post-IDPN treatment (arrowheads). Orthogonal projection showing traced HCs (asterisks) 180 days post-damage.

(H) Quantification of traced HCs.

Student's t test (C), one-way ANOVA with Tukey's multiple comparisons test (F and H), n for animals (C) and utricles (F and H). **p < 0.01, ***p < 0.001. Data are shown as mean ± SD.

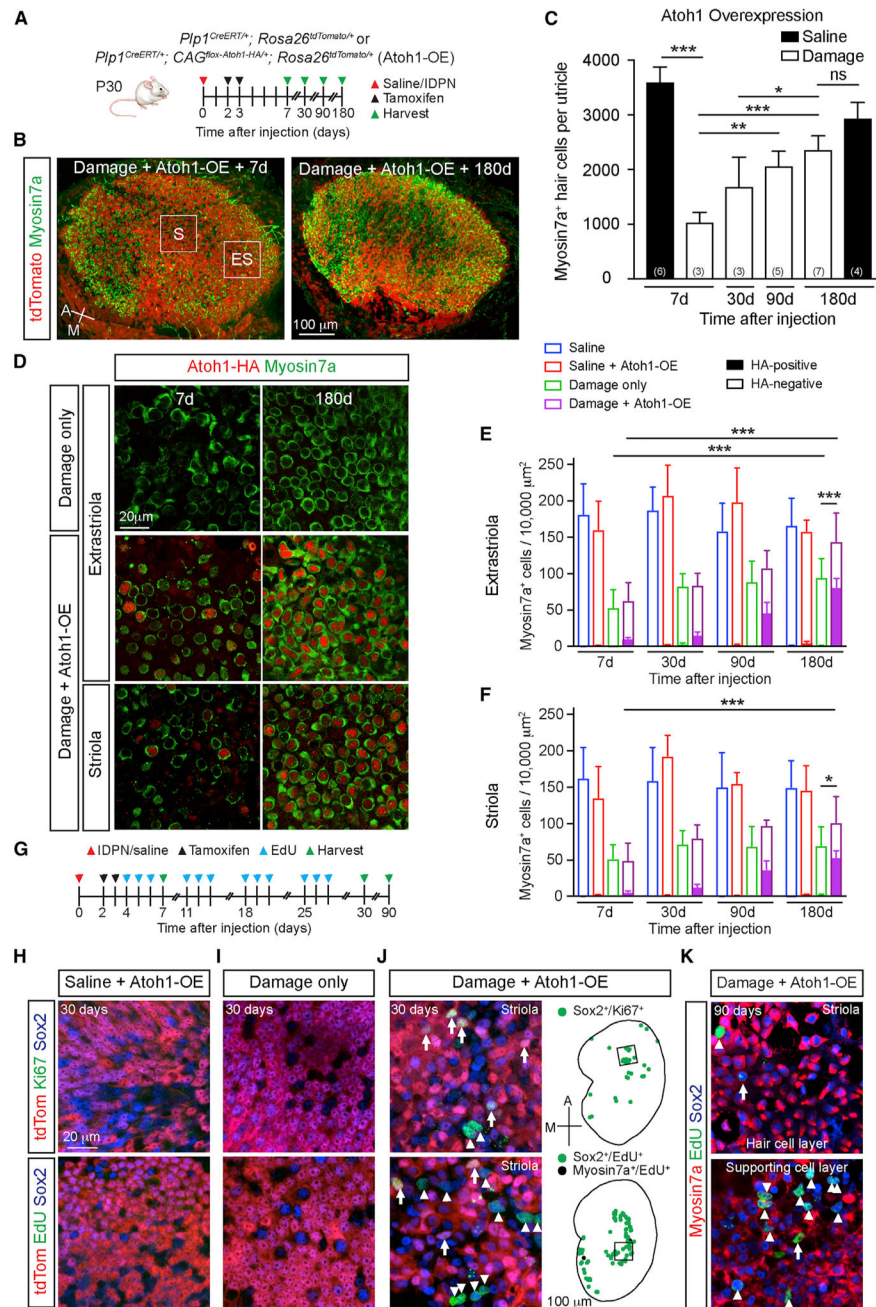


Figure 2. Atoh1 OE Enhances HC Regeneration and Proliferation

(A) Schematic for tracing and Atoh1 OE in $Plp1^+$ support cells. Atoh1 OE cells were detected via tdTomato/HA labeling.

(B) Robust repopulation of Atoh1 OE, damaged utricles with tdTomato⁺ HCs. Boxes represent extrastriolar and striolar regions where high-magnification images were taken.

(C) Quantification of total HCs post-treatment (IDPN or saline) and Atoh1 OE.

(D) Representative images of the extrastriola and striola after damage alone or with Atoh1 OE. No HA⁺ cells were identified after damage alone. HA⁺ HCs were detected after damage and Atoh1 OE.

(E and F) Extrastriolar (E) and striolar (F) HC density in undamaged, damaged only, Atoh1 OE, undamaged, and Atoh1 OE, damaged tissues. (G) Schematic to ablate HCs, fate-map Plp1⁺ support cells, and Atoh1 OE. EdU was given to label mitotic cells.

(H and I) No Ki67⁺ or EdU⁺ cells were detected in the sensory epithelium of either Atoh1 OE, undamaged (H) or damage-only (I) utricles at 30 days.

(J) Ki67⁺ and EdU⁺ support cells were detected 30 days after damage and Atoh1 OE, particularly in the striola. tdTomato-positive (arrow) and tdTomato-negative (arrowheads) proliferative (Ki67⁺ or EdU⁺) cells. Drawings depicting location of proliferative Sox2⁺ (green) and Myosin7a⁺ (black) cells; black boxes represent striolar regions where images were captured.

(K) Ninety days after damage and Atoh1 OE, many EdU⁺ cells were still detected in the striola, consisting of EdU⁺/Sox2⁺/Myosin7a⁻ support cells (arrowheads) and EdU⁺/Sox2⁺/Myosin7a⁺ HCs (arrows).

One-way ANOVA with Tukey's multiple comparisons test (C), two-way ANOVA with Tukey's multiple comparisons test (E and F), n for utricles. *p < 0.05; **p < 0.01, ***p < 0.001. Data are shown as mean ± SD.

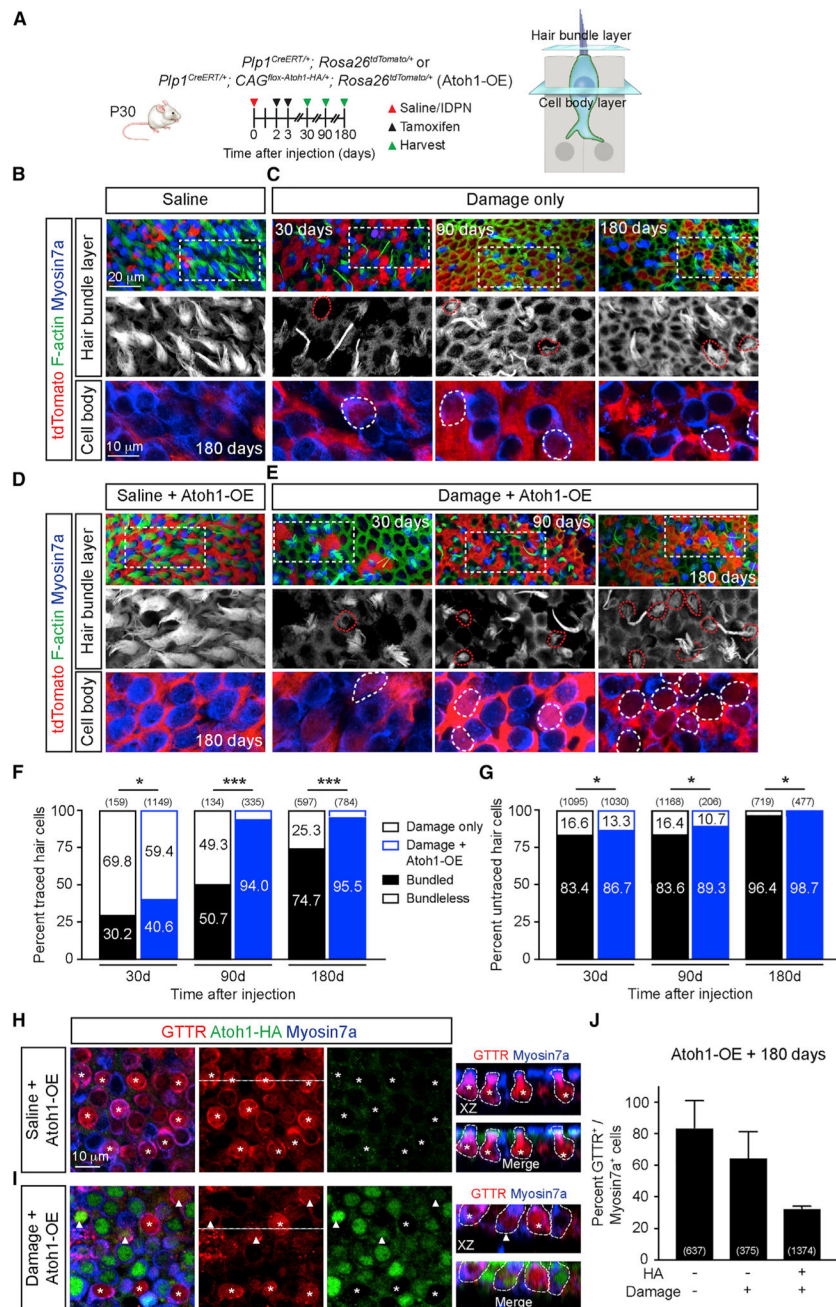


Figure 3. Atoh1 OE Enhances Stereociliary Bundle Formation

(A) Schematic showing the strategy for ablating HCs, tracing and Atoh1 OE in *Pip1*⁺ support cells. *Pip1*^{CreERT⁺}; *Rosa26*^{tdTomato/+} mice served as controls.

(B) Undamaged utricles contained many HCs with healthy and long bundles and no traced HCs. Dashed boxes represent areas from which high-magnification images at the hair bundle and cell body levels are shown.

(C) Thirty days after damage, many HCs were lost, and the few traced HCs (dashed lines) present displayed no stereociliary bundles. Ninety and 180 days after damage, more traced HCs appeared, many displaying stereociliary bundles.

(D) Atoh1 OE, undamaged control utricle show normal HC density and bundle morphology. (E) With damage and Atoh1 OE, many more traced HCs (dashed lines) gradually appeared, most noticeably at 90 and 180 days. Bundles were detected in most traced HCs. (F and G) Percentage of traced (F) and untraced (G) HCs in damage-only and Atoh1 OE, damaged utricles displaying stereociliary bundles months after damage. (H and I) Representative images of Atoh1 OE, undamaged (H) and damaged (I) utricles at 180 days. Utricles were incubated with GTTR. In undamaged tissues, all HCs were negative for HA, and most were GTTR⁺ (asterisks). With damage and Atoh1 OE, GTTR labeling was observed in Myosin7a⁺/HA⁺ (arrowheads) and Myosin7a⁺/HA HCs (asterisks). (J) Quantification of Myosin7a⁺/GTTR⁺ HCs in Atoh1 OE, undamaged and damaged utricles at 180 days. χ^2 test, n for HCs. *p < 0.05; **p < 0.01, ***p < 0.001. Data are shown as mean \pm SD.

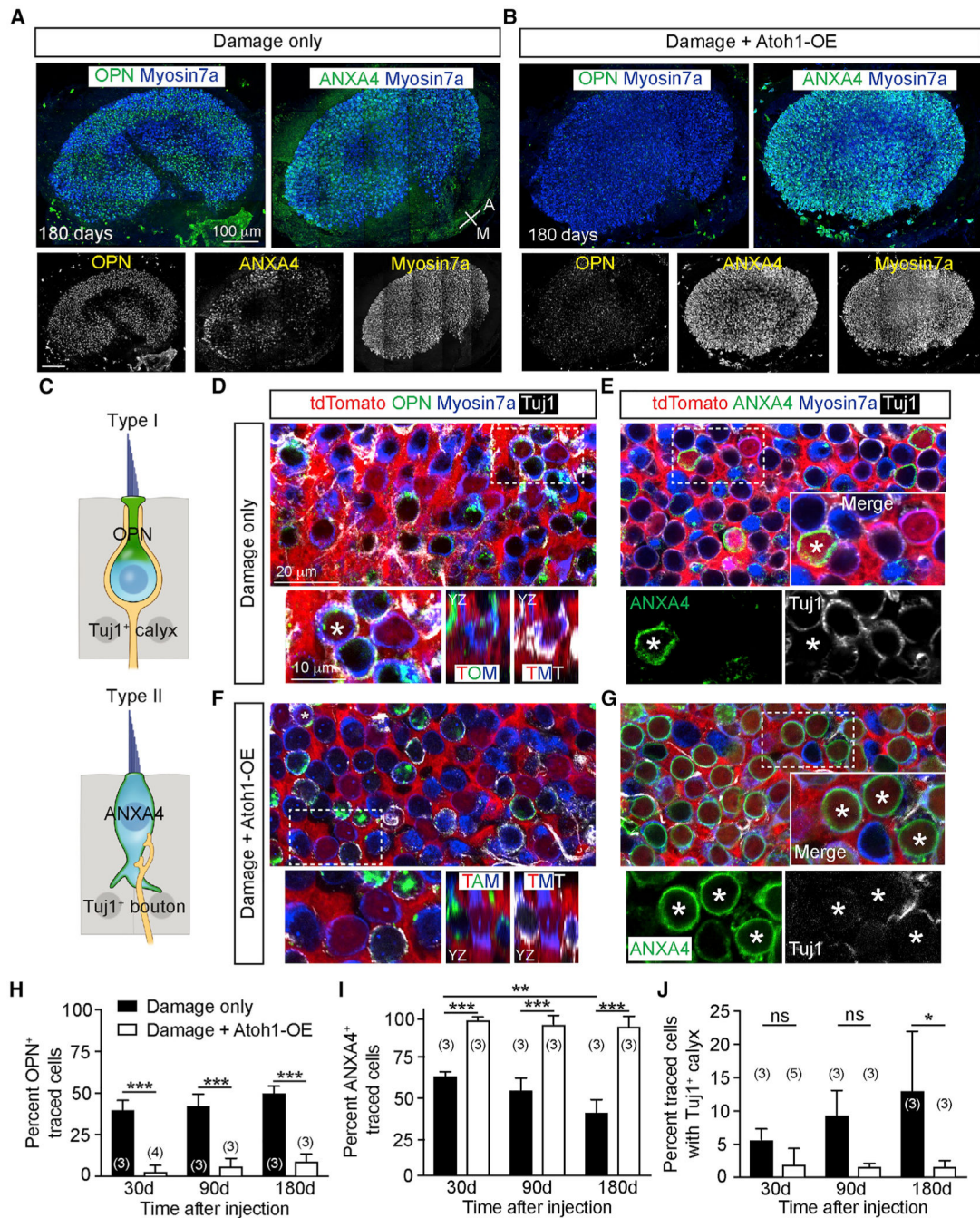


Figure 4. Atoh1 OE Increases Regeneration of Neurally Integrated Type II HCs

(A and B) Damaged-only (A) and Atoh1 OE, damaged (B) utricles demonstrating osteopontin⁺ (OPN) type I HCs and annexin A4⁺ (ANXA4) type II HCs. After damage and Atoh1 OE, the utricle was densely populated by HCs, with a noticeable loss of OPN expression.

(C) Diagram depicting amphora-shaped type I HCs expressing OPN in the neck region and goblet-shaped type II HCs expressing membranous ANXA4.

(D) Representative images of damaged utricles at 180 days showing traced, Myosin7a⁺, OPN⁺ type I HCs (asterisk) with Tuj1⁺ calyx (orthogonal view highlighting OPN and Tuj1 labeling). Traced HCs negative for OPN were also noted.

(E) Many traced Myosin7a⁺, ANXA4⁺ type II HCs (asterisk) without Tuj1⁺ calyces were found, alongside traced HCs negative for ANXA4.

(F) After damage and Atoh1 OE, there was a noticeable loss of OPN expression and Tuj1⁺ calyces among traced Myosin7a⁺ HCs (orthogonal view illustrating loss of OPN labeling). A rare traced Myosin7a⁺, OPN⁺ type I HC (asterisk) identified with a Tuj1⁺ calyx.

(G) Most traced Myosin7a⁺ HCs expressed ANXA4 without Tuj1⁺ calyces. High-magnification images showing traced HCs expressing ANXA4⁺ (asterisks).

(H–J) Quantification of traced HCs expressing OPN (H), ANXA4 (I), and displaying calyces (J).

Two-way ANOVA with Tukey's multiple comparisons test, n for utricles. *p < 0.05; **p < 0.01, ***p < 0.001. Data are shown as mean ± SD.

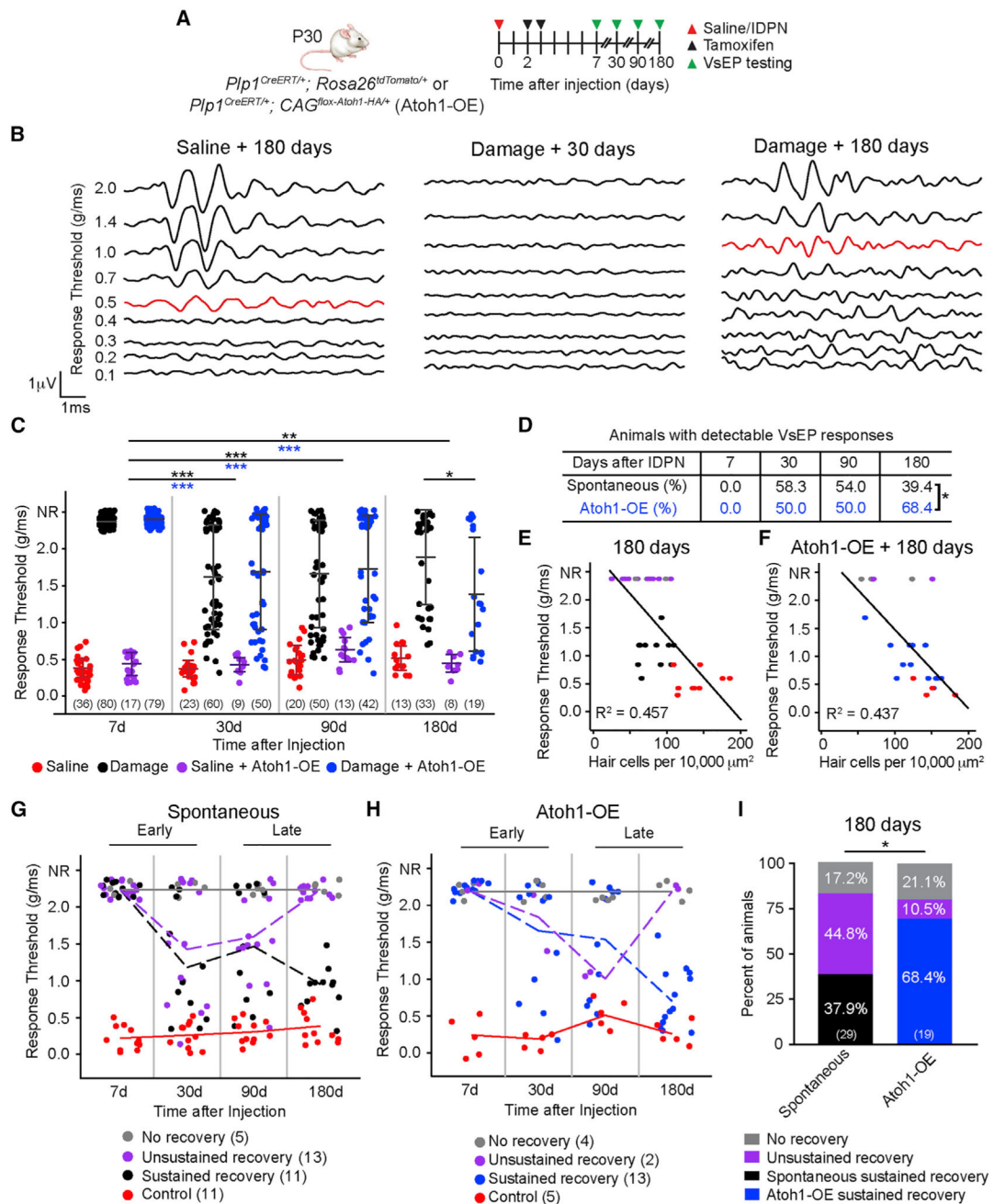


Figure 5. Atoh1 OE Enhances Functional Recovery of the Damaged, Mature Utricle

(A) Schematic showing experiments measuring VsEPs in control and damaged mice with and without Atoh1 OE.

(B) Representative VsEP traces of control animals 180 days after saline treatment (threshold 0.5 g/ms, red) and animals 30 (no responses) and 180 days after IDPN treatment (threshold 1.0 g/ms, red).

(C) VsEP thresholds of saline-treated (red), damage-only (black), Atoh1 OE, saline-treated (purple), and Atoh1 OE, damaged (blue) animals.

(D) Percentage of animals with detectable VsEP responses.

(E and F) Significant correlation between VsEP thresholds of damage-only (E) and Atoh1 OE, damaged (F) animals and utricular HC density at 180 days post-treatment.

(G) Serial measurements of individual animals show three patterns: no recovery (gray), unsustained recovery (purple), and sustained recovery (black). Control animals in red.

(H) Serial measurements of individual animals show three patterns: no recovery (gray), unsustained recovery (purple), and sustained recovery (blue). Control animals in red.

(I) Percentage of animals in each recovery group at 180 days after IDPN treatment.

Two-way ANOVA with Tukey's multiple-comparisons test (C), χ^2 test (D and I), linear regression for Pearson correlation coefficient (E and F), n for animals. *p < 0.05; **p < 0.01, ***p < 0.001. Data are shown as mean \pm SD.

KEY RESOURCES TABLE

REAGENT or RESOURCE	SOURCE	IDENTIFIER
Antibodies		
Myosin7a	Proteus Biosciences	Cat Num 25-6790; RRID:AB_2314839
Myosin7a	DSHB	Cat Num MY07A 138-1; RRID:AB_2282417
Sox2	Santa Cruz Biotechnology	Cat Num sc-17320; RRID:AB_2286684
AnnexinA4	R&D Systems	Cat Num AF4146; RRID:AB_2242796
Osteopontin	R&D Systems	Cat Num AF808; RRID:AB_2194992
Tuj1	Neuromics	Cat Num MO15013; RRID:AB_2737114
Neurofilament	Abcam	Cat Num ab4680; RRID:AB_304560
Ctbp2	BD Transduction Laboratories	Cat Num 612044; RRID:AB_399431
Shank1	Santa Cruz Biotechnology	Cat Num sc-23543; RRID:AB_2301736
Ki67	Abcam	Cat Num ab16667; RRID:AB_302459
Atoh1	Proteintech	Cat Num 21215-1-AP; RRID:AB_10733126
HA	Sigma-Aldrich	Cat Num ab9110; RRID:AB_307019
Alexa Fluor donkey anti-goat 488	Thermo Fisher Scientific	Cat Num A11055; RRID:AB_2534102
Alexa Fluor donkey anti-goat 546	Thermo Fisher Scientific	Cat Num A11056; RRID:AB_142628
Alexa Fluor donkey anti-goat 647	Thermo Fisher Scientific	Cat Num A21447; RRID:AB_141844
Alexa Fluor donkey anti-mouse 488	Thermo Fisher Scientific	Cat Num A21202; RRID:AB_141607
Alexa Fluor donkey anti-mouse 546	Thermo Fisher Scientific	Cat Num A10036; RRID:AB_2534012
Alexa Fluor donkey anti-mouse 647	Thermo Fisher Scientific	Cat Num A31571; RRID:AB_162542
Alexa Fluor donkey anti-rabbit 488	Thermo Fisher Scientific	Cat Num A21206; RRID:AB_2535792
Alexa Fluor donkey anti-rabbit 546	Thermo Fisher Scientific	Cat Num A10040; RRID:AB_2534016
Alexa Fluor donkey anti-rabbit 647	Thermo Fisher Scientific	Cat Num A31573; RRID:AB_2536183
Phalloidin	Thermo Fisher Scientific	Cat Num A22287; RRID:AB_2620155
DAPI	Thermo Fisher Scientific	Cat Num D1306; RRID:AB_2629482
Chemicals, Peptides, and Recombinant Proteins		
3,3'-iminodipropionitrile	Pfaltz & Bauer	#I00455
Tamoxifen	Sigma-Aldrich	#T5648-1G
EdU	Thermo Fisher Scientific	#A10044
NaOH	Thermo Fisher Scientific	S318-500
Tris-HCl	Thermo Fisher Scientific	#15568025
Ketamine	Vedco	#NDC 50989-161-06
Xylazine	Santa Cruz Animal Health	#SC-36294Rx
Critical Commercial Assays		
Alexa Fluor 647 EdU Detection Kit	Thermo Fisher Scientific	#C10340
Experimental Models: Organisms/Strains		
Mouse: B6.Cg-Tg(Plp1-cre/ERT)3Pop/J	Jackson Laboratory	RRID:IMSR_JAX:005975
Mouse: B6;129S6-Gt(ROSA)26Sortm14(CAG-tdTomato)Hze/J	Jackson Laboratory	RRID:IMSR_JAX:007908
Mouse: CAG-flox-Atoh1-HA	Liu et al., 2012	n/a

REAGENT or RESOURCE	SOURCE	IDENTIFIER
Antibodies		
Mouse: Cri:CD1(ICR)	Charles River	RRID:IMSR_CRL:22
Oligonucleotides		
5'-ACGCTCTGTCGGAGTTGCTG-3'	n/a	Atoh1-HA transgene (forward)
5'-AGGGATAGCCCGCATAGTCA-3'	n/a	Atoh1-HA transgene (reverse)
5'-CTAGGCCACAGAAATTGAAAGATCT-3'	n/a	Plp1-Cre internal positive control (forward)
5'-GTAGGTGGAATTCTAGCATCC-3'	n/a	Plp1-Cre internal positive control (reverse)
5'-GCGGTCTGCCAGTAAAACTATC-3'	n/a	Plp1-Cre transgene (forward)
5'-GTGAAACAGCATTGCTGTCACTT-3'	n/a	Plp1-Cre transgene (reverse)
5'-CTGTTCTGTACGGCATGG-3'	n/a	tdTomato mutant (forward)
5'-GGCATTAAAGCAGCGTATCC-3'	n/a	tdTomato mutant (reverse)
5'-AAGGGAGCTGCAGTGGAGTA-3'	n/a	tdTomato wild type (forward)
5'-CCGAAAATCTGTGGGAAGTC-3'	n/a	tdTomato wild type (reverse)
Software and Algorithms		
Fiji V2.0.0	NIH	n/a
GraphPad Prism v7.0c	GraphPad	n/a
RStudio v0.99.891	RStudio, Inc.	n/a
Other		
PBS	Sigma-Aldrich	#T5648-1G
BSA	Thermo Fisher Scientific	#BP1600-100
Na ₃	Sigma-Aldrich	#S2002-25G
DAKO	Agilent	#S3023